Impact Kinematics of Cyclist and Head Injury Mechanism in Car-to-Bicycle Collision

Tadasuke Katsuhara, Hiroshi Miyazaki, Yuichi Kitagawa, Tsuyoshi Yasuki

Abstract The number of cyclist fatalities is the third highest in traffic accidents in Japan, preceded by pedestrians and car occupants. The head is the most frequently injured body region in fatal cases. No injury assessment tests have been established for cyclist protection while impactor tests are regularly conducted for pedestrian protection. One of the reasons is that impact kinematics and injury mechanism of cyclists are not well understood. This study conducted car-to-bicycle collision simulations using finite element models for investigating head kinematics up to the contact with the car body. First, four collision cases were simulated with two car body types and two different impact locations. Impact kinematics of the cyclist was compared among the cases. The cyclist commonly showed an inclined trajectory against the car longitudinal line but the later direction changed in the SUV cases. Next, a parametric study was conducted assuming various car speed, bicycle speed, impact direction and impact position. The head reached the windshield glass and the A-pillar in the sedan cases, while it impacted the rear end of the hood and the A-pillar in the SUV cases. When the head impacted such windshield frames, the model indicated high risks of skull fracture and brain injury.

Keywords car-to-bicycle collision, human FE model, head injury, skull fracture, diffuse axonal injury

I. INTRODUCTION

Based on the traffic accident statistical data in Japan, the number of cyclist fatalities is the third highest, preceded by pedestrians and car occupants. Recently the percentage of cyclist fatalities among all deaths is increasing, in spite of the decrease of pedestrian and occupant fatalities. In the cyclist fatality cases, the most frequently injured region is the head (63%). The most frequent injury source is the ground (38%); next is the windshield frame in including the A-pillar (25%) [1]. A similar trend is observed in Europe. Fredriksson et al. investigated the bicycle accident data in Germany. They reported that head injury was frequent and was almost at the same frequency with leg injury among AIS3+ cases. The cowl, A-pillar and roof front edge, and the surroundings of windshield were the most common sources of head injury (23%), and the ground was the second most common (14%) [2]. Depreitere et al. investigated the clinical data of head injuries (AIS3+) in car-to-bicycle accident in Germany. They noted 54.2% of brain injury as well as skull fracture (80%) [3]. Skull fracture per se is not life-threatening while severe brain injury can be a direct cause of death. Studies were conducted to compare impact kinematics between pedestrians and cyclists. Margriet et al. used a pedestrian dummy to measure impact responses of pedestrians and cyclists in car collisions. They indicated that the head impact position of a cyclist was further rearward than that of a pedestrian [4]. A technical challenge in dummy testing is stabilizing the posture before impact. A common method in pedestrian dummy tests is to hold the head with a wire suspended from the ceiling and to release it at the timing of impact. However in cyclist tests, it is difficult to control the dummy and bicycle before the impact. Recent studies use computer simulation to analyze impact response of cyclists in car-to-bicycle collisions. Maki et al. compared impact kinematics of pedestrians and cyclists using a rigid link model. They reported that the cyclist had a chance to slip off from the hood due to the initial travel speed while the pedestrian fell down toward the hood at the initial impact position. The calculated wrap around distance (WAD) of the cyclist was approximately 1.2 times greater than that of the pedestrian in their cases [5]. Bellogi et al. investigated the relationship between car body shape (windshield geometry of the Mini-van) and cyclist head injury risk using a finite element (FE) model of Hybrid III AM50 dummy. They saw relatively high head injury criterion (HIC) values when the head impacted the lower end of the windshield which had relatively high stiffness compared to the other parts [6]. These studies included useful

Tadasuke Katsuhara, Ph. D. and H. Miyazaki are Assistant Managers and Y. Kitagawa, Ph. D. is Manager of Impact Biomechanics Group, Advanced CAE Division in Toyota Motor Corporation. T. Yasuki is Project General Manager of Advanced CAE Division in Toyota Motor Corporation.

information for understanding impact responses of the cyclist and skull fracture risks. However, little information was available regarding the brain injury risk. The impact conditions such as speed, direction, position etc were limited.

This study used Total Human Model for Safety (THUMS) Version 4, which enables analysis of the risk of brain injury as well as bony fractures. A common situation was assumed that a bicycle was hit by a car while crossing the road. Two car body types were considered for the striking car: sedan and SUV. First, impact responses of the cyclists were compared between the two car body types. Another simulation was conducted at a different (first) impact location for each car body type. Next, a total of 400 cases were simulated with various parameters such as car speed, bicycle speed, impact direction and impact position for each car body type. The study examined the relationship among the impact kinematics, head impact positions, skull fracture risk and brain injury risk with the parameters described above. The world's fourth fastest supercomputer "K computer" was used for performing the 800 cases in the large parametric study.

II. METHODS

Car-to-Bicycle Collision Simulation Model

Fig. 1 shows the FE models used for simulating car-to-bicycle collisions. The first car FE model represented a midsize sedan while the other car FE model represented a midsize SUV. The SUV FE model was the same as the model which was verified comparing its impact kinematics and responses with those of post mortem human subjects by Watanabe et al. [7]. The sedan FE model was constructed in a similar way to the SUV model. The height of the front edge of the hood from the ground was 790 mm in the sedan while it was 890 mm in the SUV. The car FE model represented the external geometry of each car body. During impact, the cyclist had a chance to contact the bumper, grill, hood, fender, windshield, A-pillar and roof header. Deformable materials such as metals and non-metals (plastics) were assumed for those front body parts while the other parts were assumed to be rigid. Each car FE model had approximately 3 million elements and 3.5 million nodes with a minimum element length of 1 mm. The bicycle FE model mimicked a city cycle with a tire diameter of 26 inches. Its saddle height was adjusted to 850 mm for an adult male cyclist. The pedals were set at the same height position with the left pedal forward. The tires, rims and main frames were assumed to be deformable and the other parts were assumed to be rigid. The bicycle FE model included approximately 17 thousand elements and 12 thousand nodes with a minimum element length of 10 mm. A midsize male person was assumed for the cyclist. The cyclist standing height was 1,750 mm, the riding height was 1,700 mm and the weight was 77.0 kg. THUMS Version 4 AM50 Occupant Model was used for representing the cyclist. The THUMS models were jointly developed by Toyota Central R&D Labs, Inc. and Toyota Motor Corporation. The Version 4 model enables simulations of brain and internal organ injuries as well as skeletal and ligament injuries. The geometry of human bony parts including internal organs was digitized from high-precision CT scan data. The anatomical structures of internal organs such as their locations and connections among them were duplicated referring to the anatomy books [8]. The material properties of tissue parts were defined assuming those of a male person in his thirties or forties based on the recent research data in the literature [9]. The cyclist model included approximately 1.7 million elements and 0.62 million nodes with a minimum element length of 3 mm. The study used the finite element solver LS-DYNA™ Version R6.1 for simulating car-to-bicycle collisions.

Simulation of Common Car-to-Bicycle Collision Cases

First, the study simulated a common situation in which a bicycle was hit by a car while crossing the road. The bicycle travel direction was perpendicular to that of the car. The car speed was 11.1 m/s (40 km/h) and the bicycle speed was 5.56 m/s (20 km/h). According to the report of the Institute for Traffic Accident Research and Data Analysis (ITARDA), approximately 90% of car-to-bicycle collisions (injured and fatal cases) occurred at a car speed of 11.1 m/s (40 km/h) and lower, and at a bicycle speed of 5.56 m/s (20 km/h) and lower. The model represented a collision case where the car hit the bicycle on the left side. The first impact position was described as the relative position of the cyclist head center of gravity (COG) against the front centerline of the car. Two cases were simulated for each car model. The head COG was located at 200 mm to the front centerline of the car (in the lateral direction) in the first case while it was at 600 mm in the other case (Fig. 2). Table I shows the simulation matrix. The car model and the bicycle model were placed at the positions just before collision with the initial speeds assumed respectively. The gravity was applied to the entire model. The ground (road) was modeled as a rigid plane assuming a friction coefficient of 0.3. The friction coefficient among the other parts was also assumed to be 0.3.

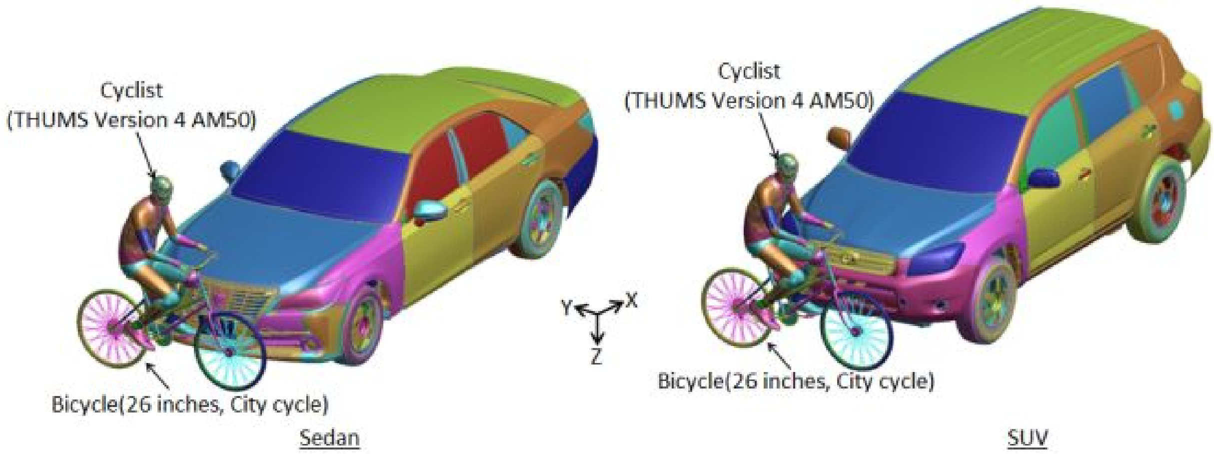

Fig. 1. Cyclist collision simulation model.

TABLE I
SIMULATION PARAMETERS

Case No	1	2	3	4
Car Type	Sedan		SUV	
Car Speed	11.1 m/s (40 km/h)	11.1 m/s (40 km/h)	11.1 m/s (40 km/h)	11.1 m/s (40 km/h)
Bicycle Speed	5.56 m/s (20 km/h)	5.56 m/s (20 km/h)	5.56 m/s (20 km/h)	5.56 m/s (20 km/h)
Impact Direction	Side	Side	Side	Side
Impact Position	600 mm	200 mm	600 mm	200 mm

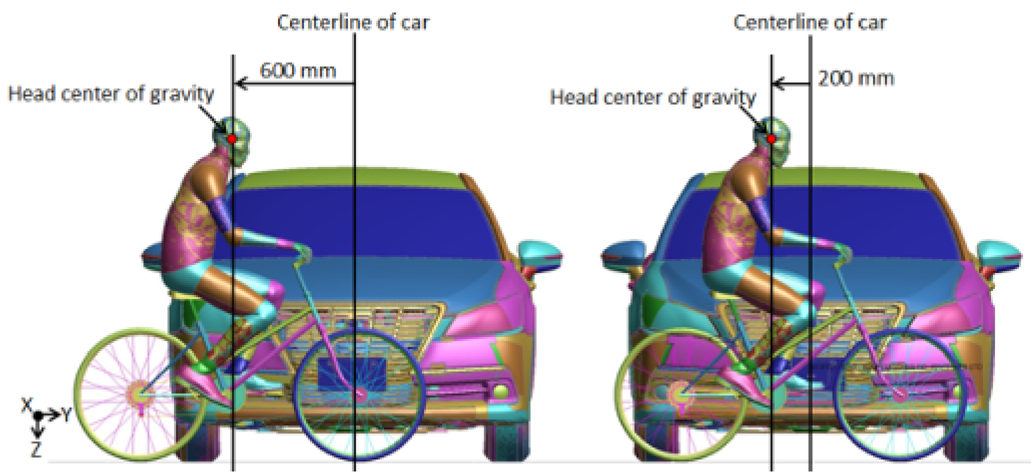

Fig. 2. Impact position (Sedan, front veiw).

Simulation of Various Car-to-Bicycle Collision Cases

Next, the study simulated car-to-bicycle collisions in various conditions. The parameters were the car body type, car speed, bicycle speed, impact direction and the impact position. Table II shows the ranges of the parameters. The car speed was changed from 2.78 m/s (10 km/h) to 16.7 m/s (60 km/h) at an interval of 2.78 m/s (10 km/h). The bicycle speed was changed from 1.39 m/s (5 km/h) to 6.94 m/s (25 km/h) at an interval of 1.39 m/s (5 km/h). The impact directions were front, lateral, rear, diagonal front and diagonal rear. The impact position was changed from -1,200 mm to 600 mm at an interval of 200 mm. Note that the negative position values mean that the bicycle passed the front centerline of the car. According to ITARDA and Maki et al, 90% of car-to-cyclist fatal accidents occur at a car speed of 16.7 m/s (60 km/h) and lower, at a bicycle speed of 6.94 m/s (25 km/h) and lower [1][5]. The impact directions were selected reflecting these accident trends. The initial impact positions were taken for the range where the car body impacted the cyclist. A total of 800 cases were conducted.

TABLE II
SIMULATION PARAMETERS FOR 800 CASES

Parameter	Variation
Car Type	Sedan, SUV
Car Speed	2.78 m/s, 5.56 m/s, 8.33 m/s, 11.1 m/s, 13.9 m/s, 16.7 m/s (10 km/h, 20 km/h, 30 km/h, 40 km/h, 50 km/h, 60 km/h)
Bicycle Speed	1.39 m/s, 2.78 m/s, 4.17 m/s, 5.56 m/s, 6.94 m/s (5 km/h, 10 km/h, 15 km/h, 20 km/h, 25 km/h)
Impact Direction	Front, Side, Rear, Diagonal Front, Diagonal Rear
Impact Position	-1,200 mm, -1,000 mm, -800 mm, -600 mm, -400 mm, -200 mm, 0 mm, 200 mm, 400 mm, 600 mm

Head Injury Index

In each case, the skull fracture risk and the brain injury risk were predicted. It was postulated that skull fracture occurred when the calculated HIC15 value exceeded 700. Although the model was capable of simulating occurrence of skull fracture by eliminating elements in the skull part, the study used HIC15 in order to estimate loading level to the head. Diffuse Axonal Injury (DAI) is one of the most severe forms of brain injury observed in traffic accidents. The risk of DAI was estimated using a strain index called Cumulative Strain Damage Measure (CSDM). The index value is the cumulative amount of volume of elements having a maximum principal strain over 25%. When the calculated CSDM value exceeded 42.5%, the model predicted the occurrence of DAI. The values were based on the research by Takhounts et al. [10]. Table III summarizes the head injury index and criterion values.

TABLE III
HEAD INJURY INDEX AND CRITERION

Parts	Injury	Index	Criterion
Skull	Fracture	HIC15	700
Brain	DAI	CDDM	42.5%

III. RESULTS

Simulation of Common Car-to-Bicycle Collision Cases

Impact Kinematics of Cyclist

Fig. 3 shows the side views of impact kinematics of the cyclists at every 40 ms in the sedan impact cases (Cases 1 and 2). The black solid line in each frame indicated the head trajectories with respect to the car. At 40 ms, the cyclist lower legs were impacted by the grill. At 80 ms, the pelvis ran up onto the hood. The lower legs kept contacting the grill. At 120 ms, the lower legs left the grill, the upper body twisted and the cyclist turned his back on the car. At 160 ms, the head impacted the car body. No significant difference in kinematics was found between Cases 1 and 2. In Case 1, the head impacted the windshield glass, while it impacted the A-pillar in Case 2. The head trajectory was straight up to 80 ms and drew an arc after that.

Fig. 4 shows the top views of impact kinematics of the cyclists at every 40 ms in the sedan impact cases (Cases 1 and 2). The black solid line in each frame indicated the head trajectories with respect to the car. In both cases, the cyclist's head moved diagonally toward the windshield glass. The trajectory lines were basically straight. After the upper body started twisting at 80 ms, the head trajectory slightly changed its direction. However, the head displacement due to the direction change was almost negligible. No significant difference in kinematics was found between Cases 1 and 2.

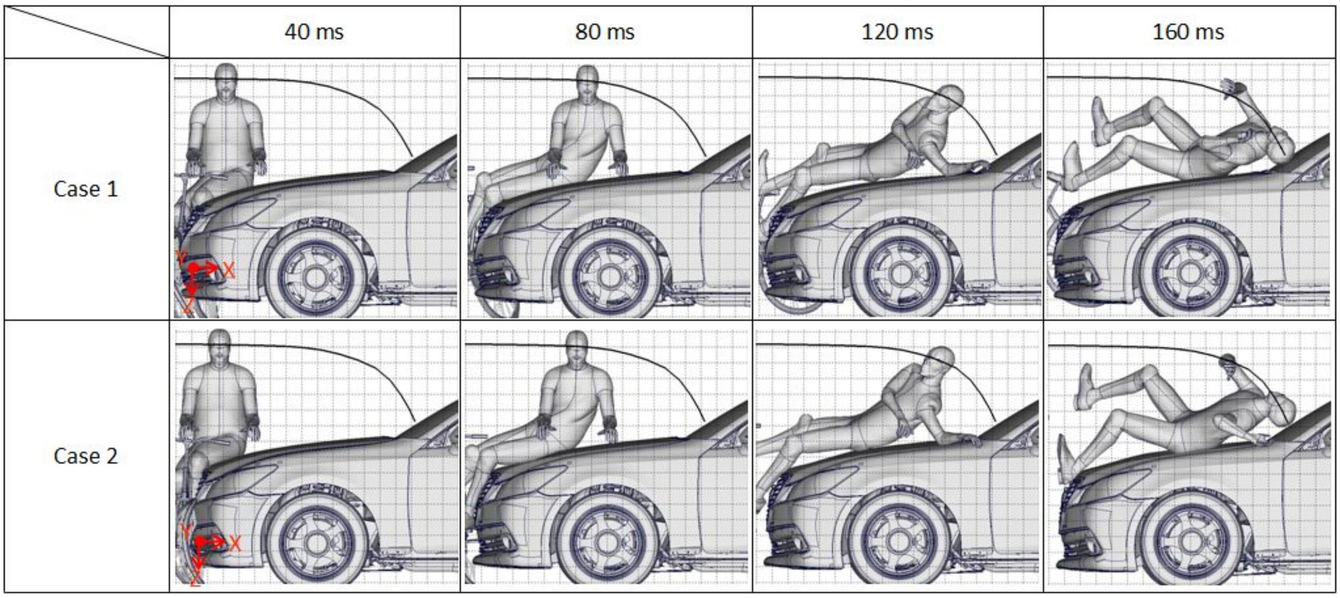

Fig. 3. Cyclist behavior with respect to the car in sedan cases (Side view).

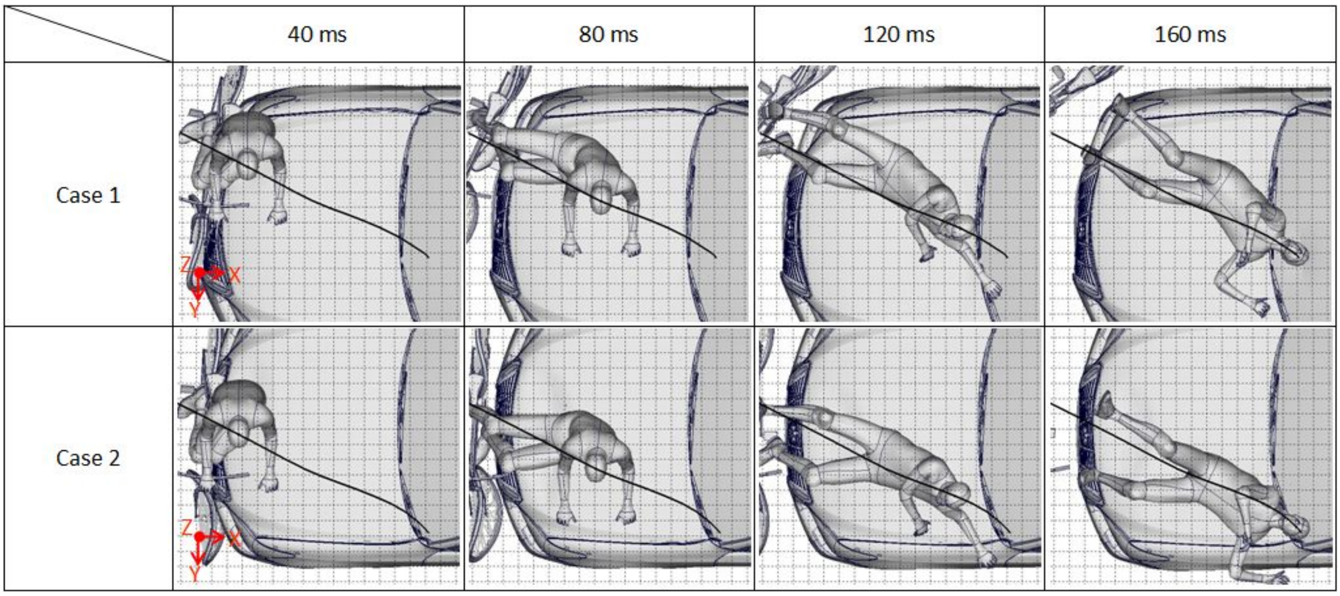

Fig. 4. Cyclist behavior with respect to the car in sedan cases (Top view).

Fig. 5 shows the side views of impact kinematics of the cyclist at 40 ms, 70 ms, 100 ms and 130 ms in the SUV impact cases (Cases 3 and 4). The black solid line in each frame indicated the head trajectory with respect to the car. At 40 ms, the cyclist lower legs were impacted by the grill. At 70 ms, the pelvis was impacted by the front end of hood. After 70 ms, the upper body rotated around the pelvis and moved toward the hood. At 100 ms, the left shoulder impacted the hood. The lower legs kept contacting the grill and the pelvis was on the hood. After 100 ms, the head rotated around the left shoulder drawing an arc. At 130 ms, the head impacted the rear end of the hood. No significant difference in kinematics was found between Cases 3 and 4. The upper body was twisted in both cases. The twisting angle was slightly greater in Case 4, but the difference in head displacement was almost negligible.

Fig. 6 shows the top views of impact kinematics of the cyclist at the same frames with Fig. 5 for Cases 3 and 4. The black solid line in each frame indicated the head trajectory with respect to the car. In Case 3, the pelvis was impacted by the head lamp. In Case 4, the pelvis was impacted by the center part of the grill and the front end of the hood. In both cases, the cyclist's head moved diagonally toward the windshield glass. The trajectory lines were almost straight up to 70 ms. After that, the head trajectory changed its direction more to rearward with the upper body twisted. This trend was commonly observed in both cases. No significant difference in kinematics was noted between Cases 3 and 4.

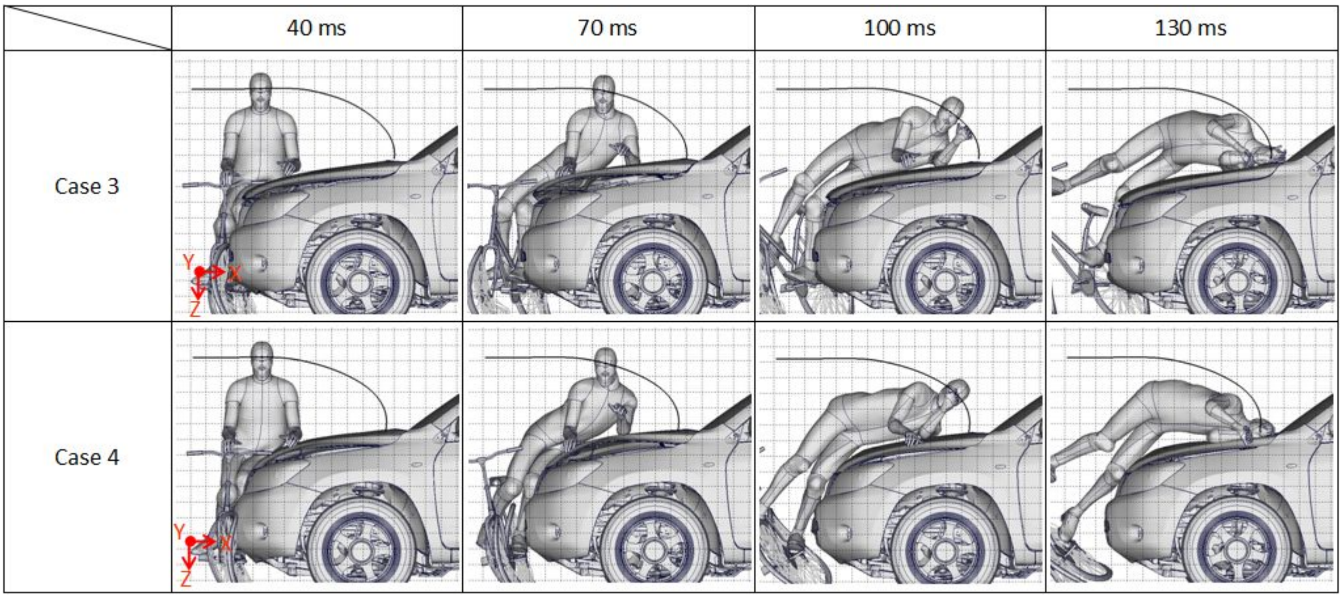

Fig. 5. Cyclist behavior with respect to the car in SUV cases (Side view).

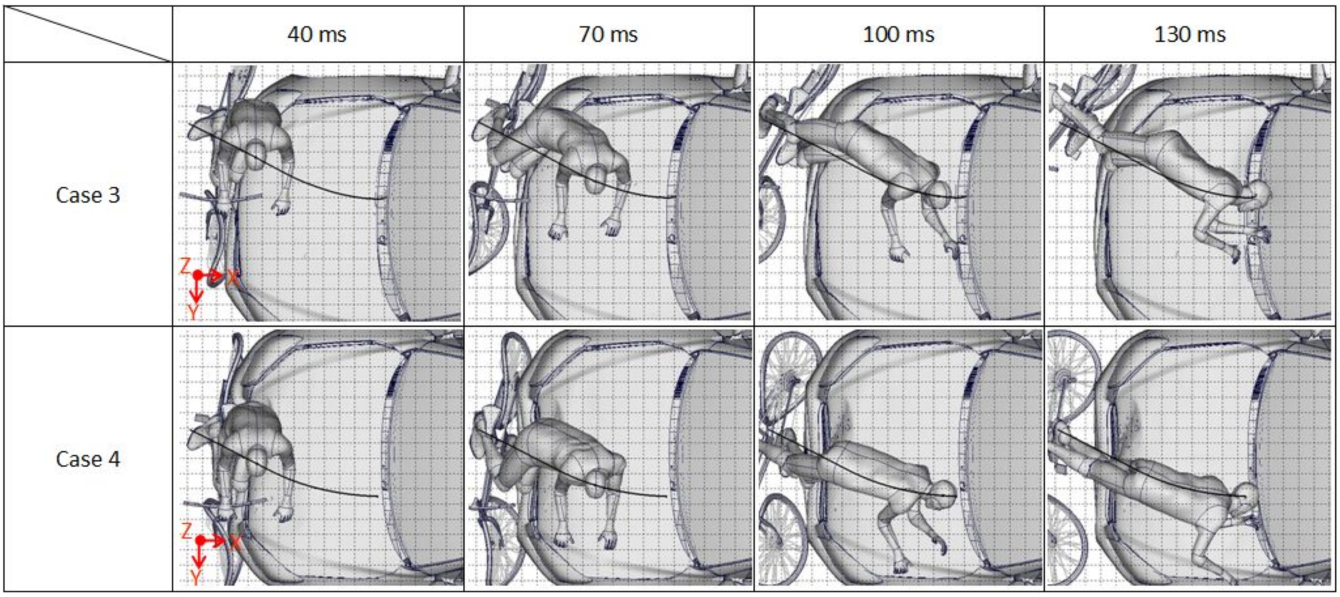

Fig. 6. Cyclist behavior with respect to the car in SUV cases (Top view).

Head Trajectory and Head Contact Point

Fig. 7 compares the head trajectories and impact points from the top views between sedan and SUV. The black solid lines indicate the head trajectories with respect to the car and the circle markers at the ends of solid lines are the head contact points. The trajectories in Cases 1 and 2 were overlaid and those in Cases 3 and 4 were overlaid. In all four cases, the trajectories had an inclination angle of 26.6 deg against the car's longitudinal line which was a resultant vector angle of car speed 11.1 m/s (40 km/h) and bicycle speed 5.56 m/s (20 km/h). In the sedan cases (Cases 1 and 2), the trajectories showed straight diagonal lines up to the head impact against the car body. In the SUV cases (Cases 3 and 4), the trajectories changed their direction more to rearward during the second half as described before. The two trajectories in each car body type showed almost the same lines with an offset due to the difference in the initial impact position. Fig. 8 shows close up views of the head contact situation in the four cases. The head reached the windshield glass in Case 1 while it impacted the A-pillar in Case 2. The head impacted the rear end of the hood in Cases 3 and 4.

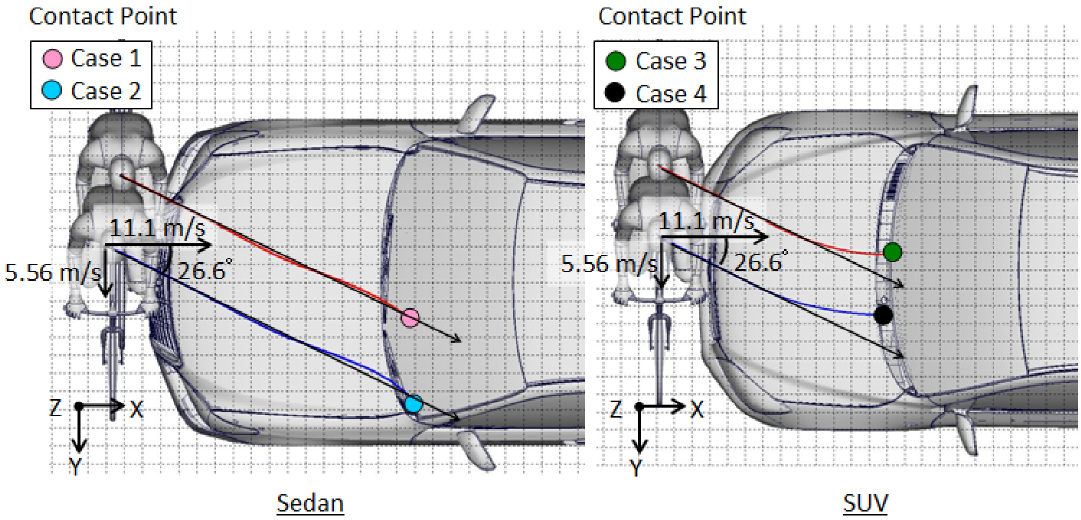

Fig. 7. Head trajectories and head contact points with respect to the car (Top view).

Case No.	1	2	3	4
Car type	Sedan		SUV	
Position	600 mm	200 mm	600 mm	200 mm
Head Contact	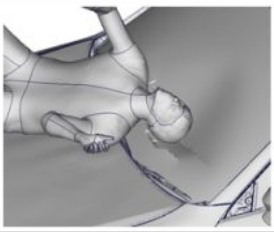	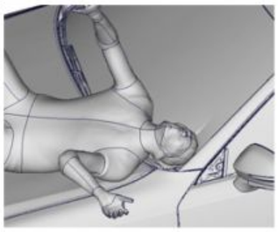	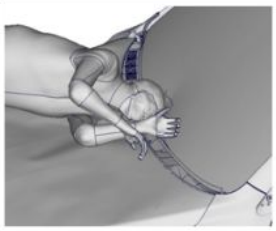	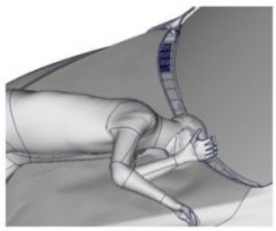

Fig. 8. Head contact situation.

Head Contact Force

Fig. 9 shows the time history curves of contact force between the cyclist's head and the car body. In Case 1 (sedan, impact position 600 mm), the force rose at 155 ms and peaked at 158 ms. In Case 2 (sedan, impact position 200 mm), the force did not rise until 168 ms and the maximum peak appeared at 176 ms. In Case 3 (SUV, impact position 600 mm), the initial rise was observed at 124 ms and the peak was noted at 134 ms. In Case 4 (SUV, impact position 200 mm), the force rose at 115 ms and peaked at 120 ms. In both sedan and SUV, the timings of head impact in the cases with an impact position of 600 mm were later than those in the cases with an impact position of 200 mm. The peak values were 2.1 kN (Case 1), 8.3 kN (Case 2), 3.9 kN (Case 3) and 4.2 kN (Case 4), respectively. The peak value of Case 1 was the lowest where the head impacted the windshield glass. The peak value of Case 2 was the highest where the head impacted the A-pillar.

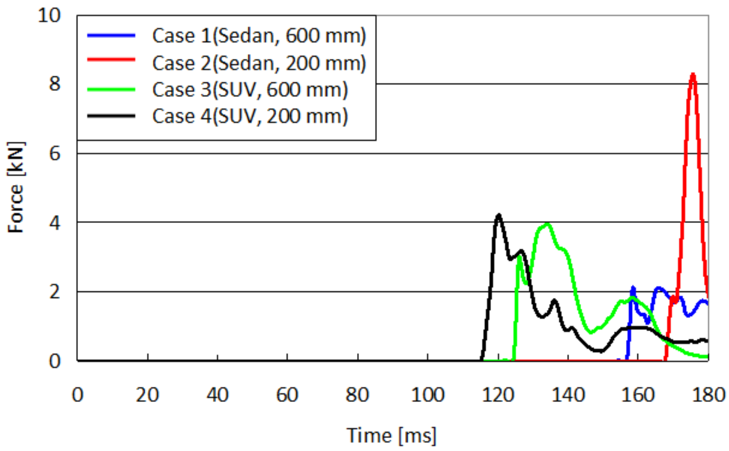

Fig. 9. Time history of head contact resultant force.

Head Velocity

Fig. 10 shows the time history curves of the head relative velocity with respect to the car body. The relative velocities were compared among the four cases for each component. The x-direction coincided with the car's longitudinal direction. The y-direction coincided with the car's width direction. The z-direction coincided with the vertical line. In the sedan cases (Cases 1 and 2), the head x-velocity started increasing at 80 ms when the pelvis ran onto the hood, but it turned to decrease at 120 ms when the upper body started twisting. Finally the relative velocity decreased to zero approximately at 180 ms. The velocity was higher in Case 2 during the latter period. In the SUV cases (Cases 3 and 4), the head x-velocity started increasing at 60 ms, peaked approximately at 80 ms and turned to decrease after that. It reached zero when the head impacted the car body at 130 ms in Case 3 and at 120 ms in Case 4. The gradients of velocity decrease curves were greater in the SUV cases compared to those in the sedan cases. In the sedan cases, the head y-velocity did not show a monotonic change but repeated up and down between 4 m/s and 5 m/s. In the SUV cases, the head y-velocity started decreasing at 40 ms and reached zero approximately at 110 ms just before the head impacted the car body. In the sedan cases, the head z-velocity started increasing at 80 ms when the pelvis ran onto the hood, peaked at 140 ms just before the head impacted the car body and decreased after that. In the SUV cases, the head z-velocity started increasing at 40 ms when the lower legs impacted the grill, peaked approximately at 110 ms just before the head impacted the car body, and decreased after that.

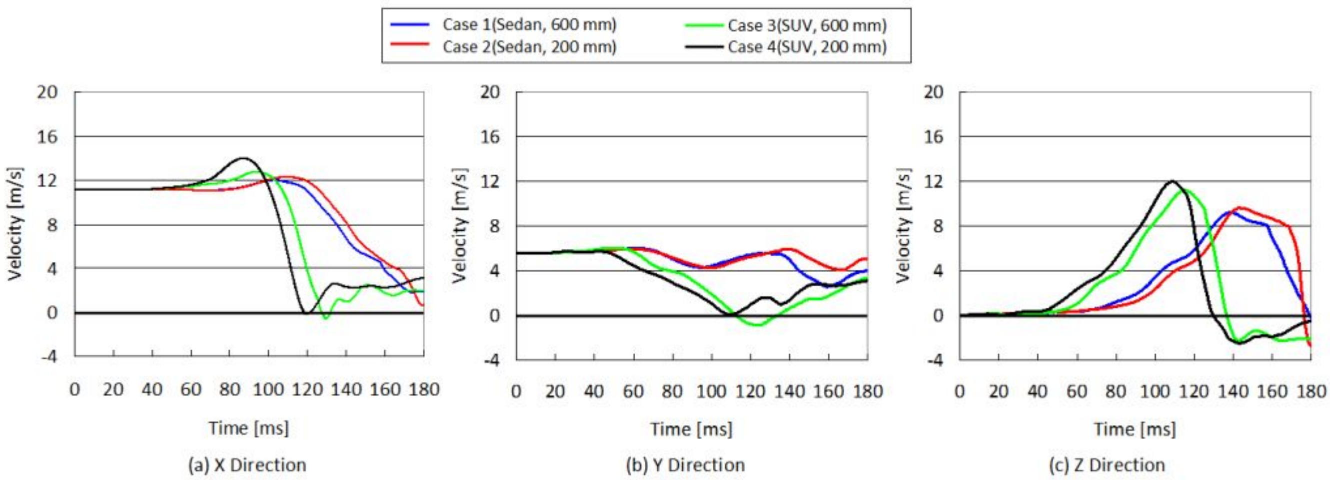

Fig. 10. Time history of head relative velocity with respect to the car.

Head Rotational Velocity and Rotational Acceleration

Fig. 11 shows the time history curves of the head rotational velocities around the COG for the four cases. In the sedan cases (Cases 1 and 2), the rotational velocity started increasing at 70 ms just before the pelvis ran onto the hood, peaked at 125 ms when the upper body started twisting. The peak values were 81 rad/s in Case 1 and 77 rad/s in Case 2. In the SUV cases (Cases 3 and 4), the rotational velocity started increasing at 60 ms just before the pelvis impacted the grill, and reached a peak of 56 rad/s at 100 ms in Case 3 and a peak of 64 rad/s at 110 ms in Case 4 before the head impacted the car body.

Fig. 12 shows the time history curves of the head rotational accelerations around the COG for the four cases. In the sedan cases, the peak appeared at 140 ms (5,300 rad/s^2) in Case 1 and at 135 ms (5,100 rad/s^2) in Case 2, before the head impacted the car body. In the SUV cases, the peak appeared at 126 ms (9,700rad/s^2) in Case 3 and at 120 ms (9,800rad/s^2) in Case 4, just after the head impacted the car body.

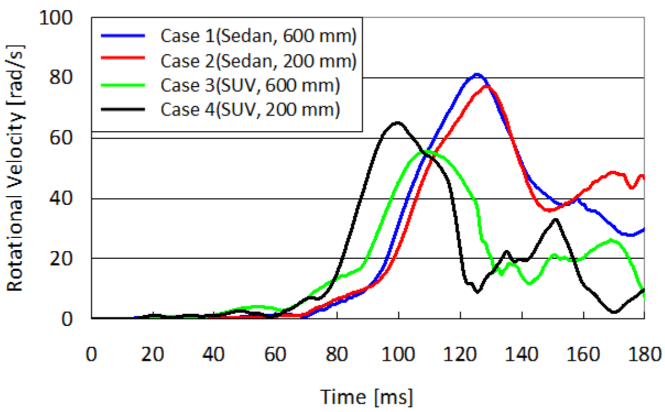

Fig. 11. Time history of head rotational velocity.

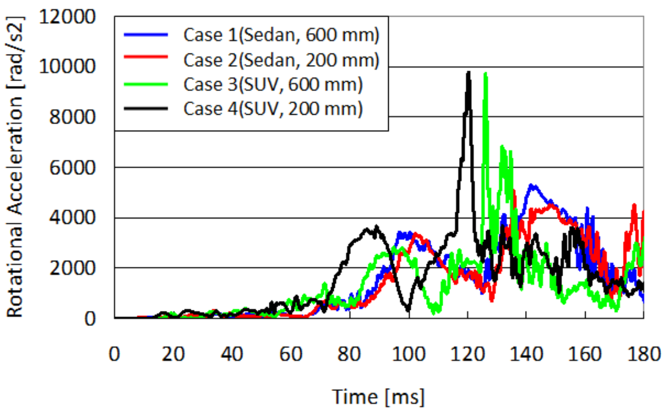

Fig. 12. Time history of head rotational acceleration.

Head Injury

Table IV shows the predicted results of head injuries. In Case 1, where the cyclist head impacted the windshield of the sedan, neither skull fracture nor DAI occurred. In Case 2, where the head impacted the A-pillar, the model predicted occurrence of skull fracture. In Cases 3 and 4 (SUV cases), where the head impacted the rear end of the hood, neither skull fracture nor DAI occurred.

TABLE IV
INJURY RESULTS

Case No		1	2	3	4
Car Type		Sedan	Sedan	SUV	SUV
Impact Position		600 mm	200 mm	600 mm	200 mm
Injury	Skull Fracture	non	Fracture	non	non
	DAI	non	non	non	non

Simulation of Various Car-to-Bicycle Collision Cases

Distribution of Head Contact Points

Fig. 13 shows the distribution of head contact points with respect to the car in 400 cases for each car body type. The head contact points were distributed not only on the car body but also on the ground. The points on the car body were found at the front part and the right lateral part, but were more concentrated at the area between the center of the hood and the windshield glass. The points on the ground were found at the front, right side and left side of the car, but more at the left side. In both sedan and SUV cases, the points on the windshield glass accounted for 40%, ground for 30%, hood for 25% and the other parts for 5%.

Fig. 14 shows the impact kinematics of the cyclist falling to the ground. The striking car was the sedan. The car speed was 11.1 m/s (40 km/h). The bicycle speed was 5.56 m/s (20 km/h). The impact position was 200 mm from the width center of car. The black solid line in each frame indicated the head trajectory with respect to the car. At 40 ms, the cyclist lower legs were impacted by the grill. At 80 ms, the pelvis ran up onto the hood. The lower legs kept contacting the grill. At 120 ms, the lower legs left the grill, the upper body twisted and the cyclist turned his back on the car. The kinematics up to this time was similar to those in Case 1 described above. At 160 ms, the head trajectory drew an arc around the pelvis. At 200 ms, the head did not impact the A-pillar but passed by. At 400 ms, the cyclist turned upside down. At 600 ms, the cyclist landed on the ground with the legs. The cyclist kept rotating and the shoulder touched the ground at 760 ms. Finally the head impacted the ground at 770 ms. The model predicted occurrence of skull fracture in this case.

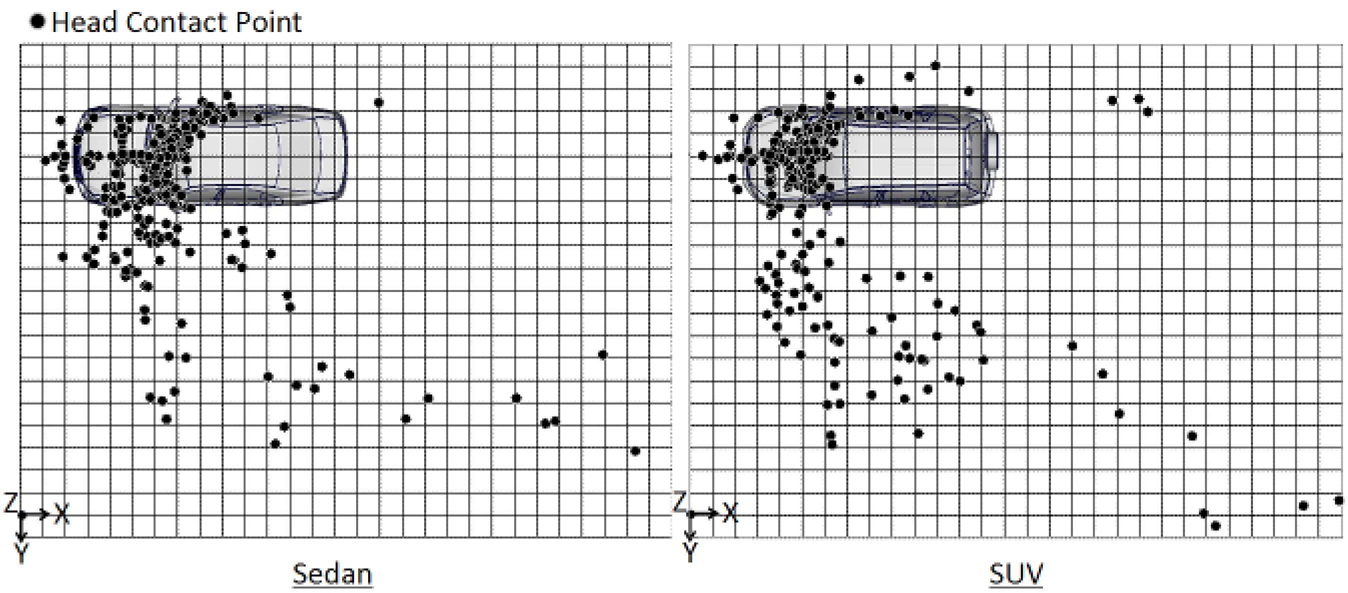

Fig. 13. Head contact points with respect to the car (800 cases).

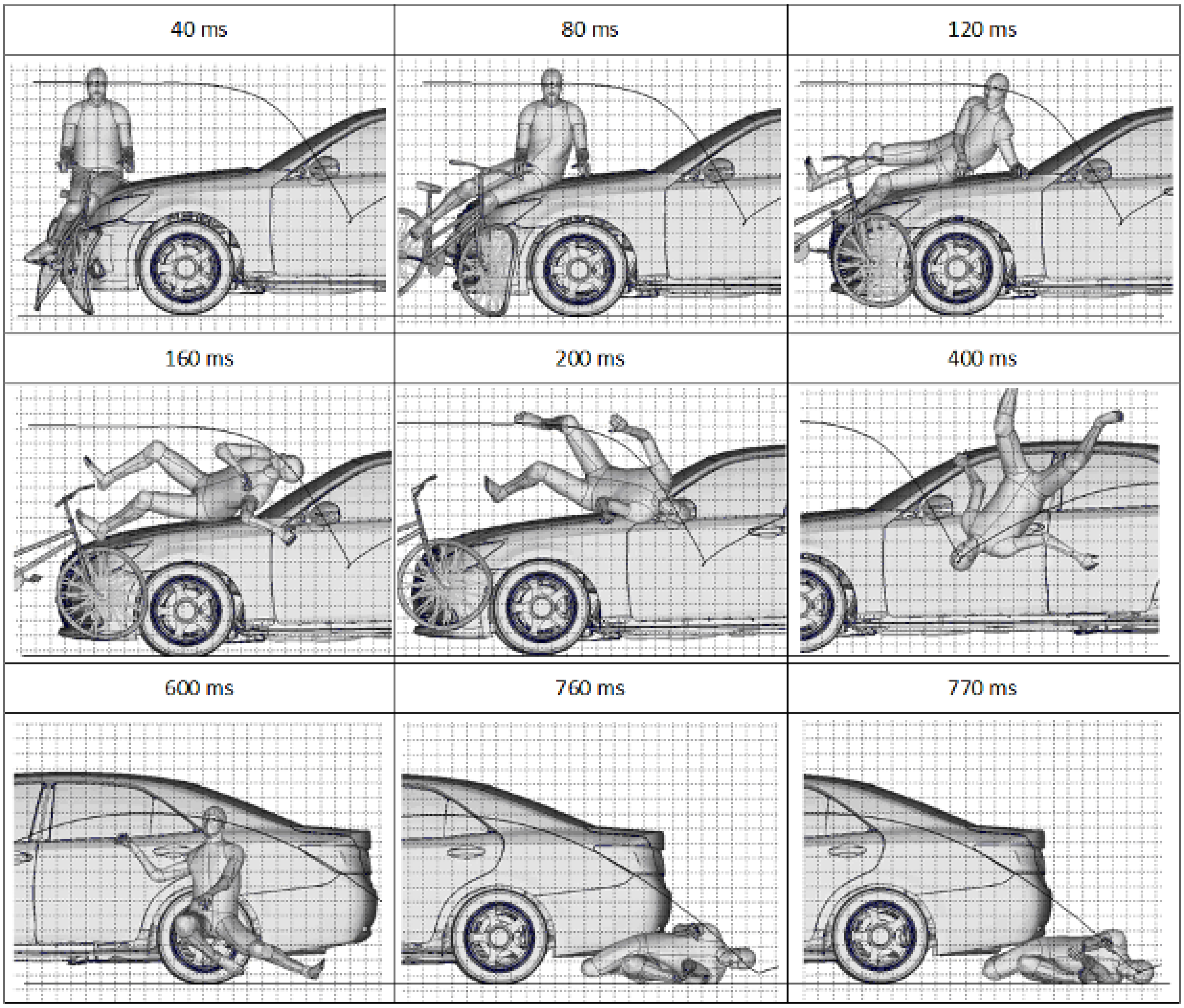

Fig. 14. Ground impact behavior with respect to the car in sedan case.

Fig. 15 shows the distribution of head contact points with corresponding HIC15 levels for the two car types. The circle marks are the head contact points and their colors indicate the HIC15 level; red is over 700, yellow is between 500 and 700, green is between 300 and 500, and blue is under 300. Skull fracture can occur at the red marks. In the sedan cases, the red marks were mostly found on the A-pillar and barely found on the header and the rear end of the hood. In the SUV cases, the red marks were distributed on the A-pillar and the rear end of the hood.

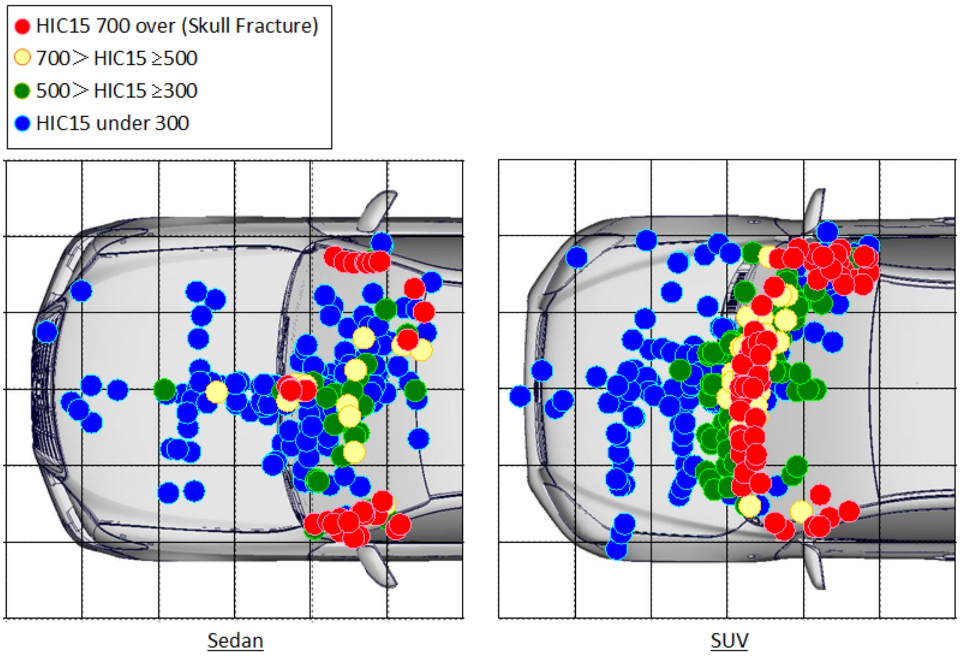

Fig. 15. Distribution of head contact points with HIC15 levels.

Fig. 16 shows the distribution of head contact points with corresponding CSDM levels for the two car types. The square marks are the head contact points and their colors indicate the CSDM level; red is over 42.5%, yellow is between 30% and 42.5%, green is between 20% and 30%, blue is under 10%. DAI can occur at the red marks. In both sedan and SUV cases, the red marks were concentrated on the upper part of the A-pillar.

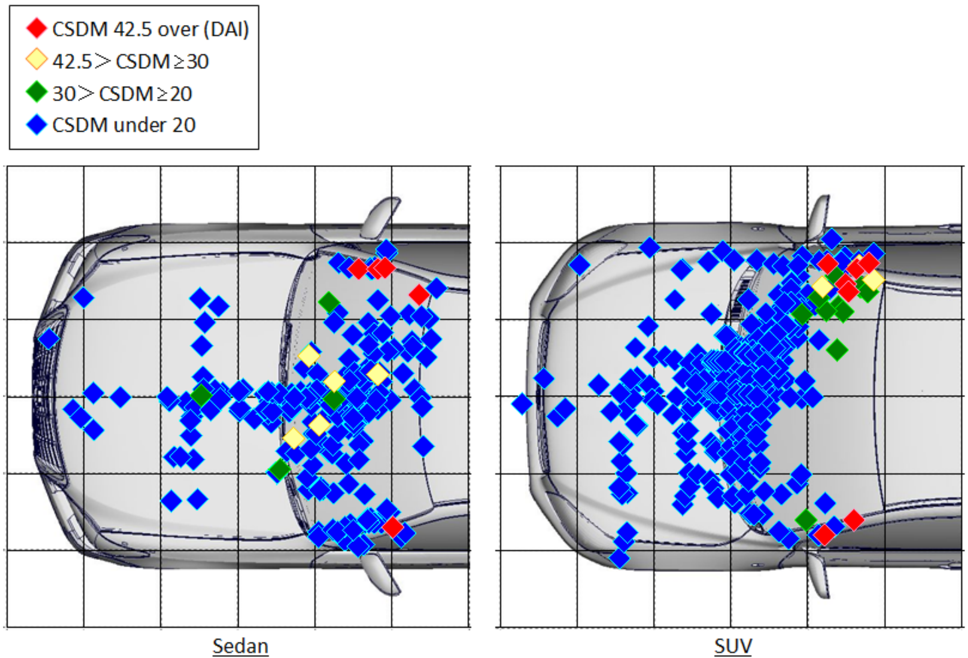

Fig. 16. Distribution of head contact points with CSDM levels.

Fig. 17 shows the percentage of HIC15 level in Fig. 15. In the sedan, HIC15 700 over: 15.4%; HIC15 between

500 and 700: 6.7%; HIC15 between 300 and 500: 11.4%; HIC15 under 300: 66.5%. In the SUV, HIC15 700 over: 19.9%; HIC15 between 500 and 700: 12.2%; HIC15 between 300 and 500: 26.6%; HIC15 under 300: 41.3%.

Fig. 18 shows the percentage of CSDM level in Fig. 16. In the sedan, CSDM 42.5% and over: 2.3%; between 30% and 42.5%: 2.3%; between 20% and 30%: 1.8%; under 20%: 93.6%. In the SUV, CSDM 42.5% and over: 2.6%; between 30% and 42.5%: 1.1%; between 20% and 30%: 3.6%; under 20%: 92.7%.

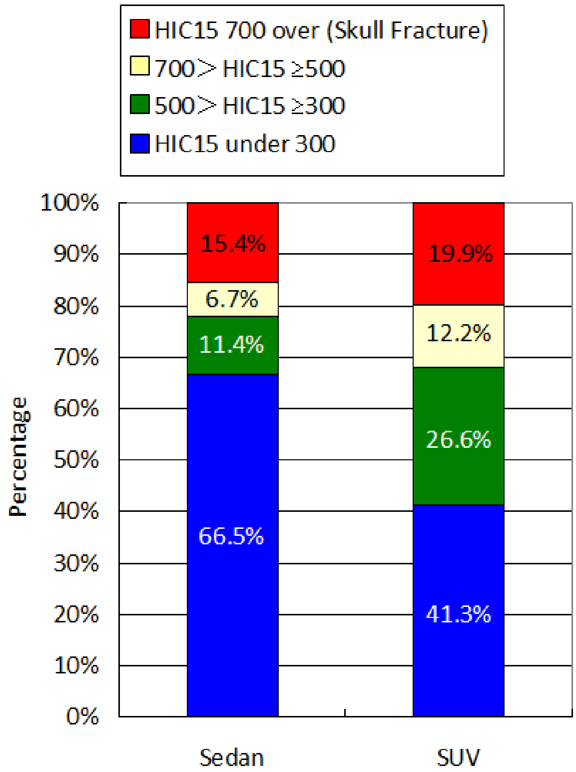

Fig. 17. Percentage of HIC15 level.

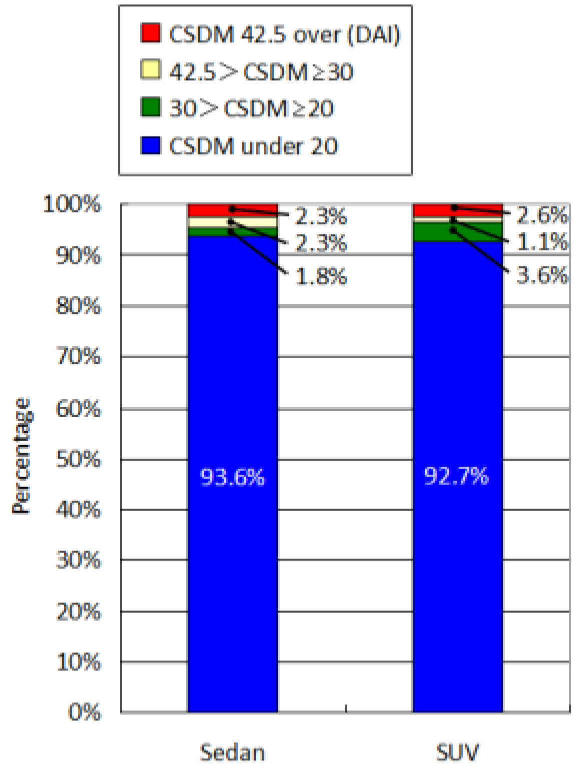

Fig. 18. Percentage of CSDM level.

Table V shows the ranges of parameters when skull fractures occurred (high HIC15 level). In both sedan and SUV cases, the car speed was equal to or higher than 8.33 m/s (30 km/h). High HIC15 values were noted at any bicycle speed. The first impact position ranged from 1,000 mm to 800 mm and from 400 mm to -400 mm in the sedan cases, while it ranged from 1,200 mm to -600 mm in the SUV cases. As for the impact direction, high HIC15 values were found in front, side and diagonal front directions in the sedan cases, while those were found in front, side, rear and diagonal front directions in the SUV cases.

Table VI shows the ranges of parameters when DAI occurred (high CSDM level). In both sedan and SUV cases, the car speed was equal to or higher than 13.9 m/s (50 km/h). High CSDM values were noted at any bicycle speed. The first impact position was limited to -800 mm and -200 mm in the sedan cases, while it scattered at -1,000 mm, -800 mm, -400 mm and -600mm in the SUV cases. As for the impact direction, high CSDM values were found in front and side directions in the sedan cases, while those were found in front, side and rear directions in the SUV cases.

TABLE V
SIMULATION PARAMETER OF HIC15 700 OVER

Car Type	Sedan	SUV
Car Speed	More than 8.33 m/s (30km/h)	More than 8.33 m/s (30km/h)
Bicycle Speed	Between 1.39 m/s and 6.94 m/s (Between 5 km/h and 25km/h)	Between 1.39 m/s and 6.94 m/s (Between 5 km/h and 25km/h)
Impact Position	Between -1,000 mm and -800 mm Between -400 mm and 400 mm	Between -1,200 mm and 600 mm
Impact Direction	Front, Side, Diagonal Front	Front, Side, Rear, Diagonal Front

TABLE VI
SIMULATION PARAMETER OF CSDM 42.5% OVER

Car Type	Sedan	SUV
Car Speed	16.7 m/s (60 km/h)	More than 13.9 m/s (50 km/h)
Bicycle Speed	Between 1.39 m/s and 6.94 m/s (Between 5 km/h and 25km/h)	Between 1.39 m/s and 6.94 m/s (Between 5 km/h and 25km/h)
Impact Position	-800 mm and -200 mm	-1,000 mm, -800 mm, 400 mm and 600 mm
Impact Direction	Front, Side	Front, Side, Rear

IV. DISCUSSION

Simulation of Common Car-to-Bicycle Collision Cases

As observed in Fig. 7, the cyclist moved diagonally from the impact position to the car body along the resultant vector of the striking car speed and the crossing bicycle speed. In the sedan cases, the trajectories showed straight diagonal lines up to the head impact against the car body. In the SUV cases, the trajectories changed their direction more to rearward approximately at 70 ms when the pelvis was impacted by the front end of the hood. It was conjectured that the upper body motion in the crossing direction was restrained due to the pelvis engagement. As a result the head trajectory changed its direction more to rearward after 70 ms in the SUV cases. In the sedan cases, the lower legs were engaged by the grill but the pelvis ran onto the hood. The lower leg engagement did not restrain the upper body motion. The head trajectory kept straight diagonal lines in the sedan cases. Such a difference in kinematics resulted in the difference in head velocity change between the two car body types as shown in Fig. 10. The head y-velocity kept a range from 4.17 m/s (15 km/h) to 5.56 m/s (20km/h) in the sedan cases while it dropped to zero in the SUV cases.

The pelvis engagement also affected the cyclist kinematics. In the sedan cases, the cyclist legs were engaged by the grill while the pelvis moved diagonally on the hood. This rotated the upper body and resulted in the face up position. In the SUV cases, the pelvis was engaged by the front edge of the hood at 70 ms. After 70 ms the upper body kept moving and flexed. The cyclist laid face down in this case. To clarify the relation between the cyclist kinematics and head injury, more investigation is necessary.

Skull fracture occurred only in Case 2 where the cyclist's head impacted the A-pillar. The head impacted the windshield glass in Case 1 and the rear end of the hood in Cases 3 and 4. Among these body parts, the A-pillar had the highest stiffness against impact followed by the rear end of the hood, and the windshield glass had the lowest stiffness. Such a difference in stiffness explains the difference in force magnitude among the cases shown in Fig. 9. The head experienced the greatest force when impacting the A-pillar in Case 2 while it was subjected to the smallest force when impacting the windshield glass. The skull fracture risk becomes higher as the force is greater. It is concluded that the distribution of head contact points was mostly correlated with the distribution of stiffness of the body parts. DAI did not occur in the four cases. The study used CSDM to predict occurrence of DAI. In general, CSDM tends to become high when the head is rotated rapidly [11]. Margulies et al. reported that DAI was likely to occur at a rotational acceleration of 8,000 rad/s^2 and higher [12]. The calculated head rotational acceleration peaks were higher than that in Case 3 (9,700 rad/s^2) and Case 4 (9,800 rad/s^2). A possible explanation is that the duration of head rotational acceleration was short in those cases (Fig. 12).

Simulation of Various Car-to-Bicycle Collision Cases

The distribution of head contact points with HIC15 levels for the 800 cases showed that the red marks were concentrated on the windshield frames in both sedan and SUV cases (Fig. 15). The results indicated relatively high risk of skull fracture when the head impacted those parts. This is consistent with the finding from the four cases described above and with the fact that, based on the accident database, fatal head injuries of cyclists were likely to be caused by impacts to the windshield frames including the A-pillar. It should be noted that the head contact points in the sedan cases were more distributed over the windshield glass including the A-pillar. Relatively few points were noted at the rear end of the hood. This is because the cyclist traveled a long distance on the hood after the pelvis ran onto the hood. The A-pillar was the stiff part in that area and was a potential source of skull fracture. The head trajectories were basically straight diagonal in the sedan cases. That is the reason why the first impact positions with high HIC15 values were separated into two ranges, corresponding to the right and left A-pillars. On the other hand, the head contact points in the SUV cases were distributed to the area from the center of the hood to the lower part of the windshield glass. The travel distance was relatively short due to the pelvis engagement. The A-pillar and the rear end of the hood were the stiff parts in that area and were potential sources of skull fracture. That is the reason why the first impact positions with high HIC15 values were distributed over a wide range in the SUV cases (Table V).

The distribution of head contact points with CSDM levels showed that the red marks appeared mostly on the upper part of the A-pillar in both sedan and SUV cases (Fig. 16). The marks on the rear end of the hood indicated relatively low CSDM level. High CSDM values were found at 16.7 m/s (60 km/h) in the sedan cases and at 13.9 m/s (50 km/h) and higher in the SUV cases (Table VI). This suggests that high kinetic energy is necessary to generate DAI. The cyclist's head reached the upper part of the A-pillar in high speed impacts. That is the reason why the high CSDM values were concentrated on that area. Watanabe et al. conducted car-to-pedestrian collision simulations and reported that DAI was likely to occur when the car speed was 11.1 m/s (40 km/h) and higher [7]. Although impact kinematics was different among pedestrians and cyclists, the two study results suggested that high impact energy generated DAI.

V. LIMITATION

The simulation models used for this study were separately validated against physical experimental data in the literature. The impact response of the head part of THUMS Version 4 AM50 Occupant Model had been validated against those of post mortem human subjects. The whole body kinematics and response had been validated against those in the car-to-pedestrian collision tests. The force deformation response of the car models had been validated against those in impactor tests. The impact response of the bicycle model was not validated. The whole body kinematics in car-to-bicycle collisions was not validated. This study used CSDM to estimate the risk of DAI. The validity of CSDM has not been fully proved. The study revealed a possible mismatch in estimating DAI between CSDM and head rotational acceleration. Further study is necessary to examine the relationship between such indicators.

VI. CONCLUSIONS

- Car-to-bicycle collision simulations were conducted using FE models. Two car body types were considered: sedan and SUV. THUMS Version 4 AM50 Occupant Model was used for representing the cyclist. The cyclist model was placed on the bicycle model representing a city cycle with a tire diameter of 26 inches. First, four common collision cases were simulated to understand the impact kinematics of the cyclist and to estimate the risk of skull fracture and DAI. Next, four hundred collision cases were simulated for each car body type changing the parameters such as car speed, bicycle speed, impact direction and impact position. The relationship between the parameters and skull fracture and DAI risks were investigated.
- The cyclist moved diagonally along the resultant vector of the striking car speed and the crossing bicycle speed. In the sedan cases, the pelvis ran onto the hood and the cyclist traveled a long distance allowing the head to reach the windshield glass. In the SUV cases, the pelvis was impacted and engaged by the front end of the hood and the upper body motion was restrained allowing smaller travel distance of the head. The head contact points were distributed to the car body and the ground. The study focused on the cases where the head impacted the car body. The head trajectories kept straight diagonal lines up to the contact in the sedan cases, while they changed the direction more to rearward due to the pelvis engagement in the SUV cases.
- When the cyclist's head impacted the A-pillar or the rear end of the hood, the contact force tended to be great increasing the HIC15 value. Skull fracture was likely to occur in such a case. In the sedan cases, high HIC15 values were mostly found at the right and left A-pillars. In the SUV cases, high HIC15 values were distributed to the A-pillars and the rear end of the hood. When the head impacted the A-pillar with high kinetic energy, the model predicted DAI with high CSDM values.

VII. ACKNOWLEDGEMENT

This study was carried out as part of Japan Automobile Manufacturers Association, Inc.'s research activities. The authors would like to thank RIKEN, Japan Automobile Manufacturers Association, Inc. and FUJITSU LIMITED.

VIII. REFERENCES

[1] ITARDA, Report of In-Depth Accident Analysis, 2012 Edition (in Japanese).

[2] Fredriksson R, Rosen E. Priorities for bicyclist protection in car impacts. A real life study of severe injuries and car sources. *Proceedings of IRCOBI Conference*, 2012, 779-786 (IRC12-83), Dublin, Ireland.

[3] Depreitere B, Lierde C, et al. Bicycle-related head injury: a study of 86 cases. *Accident Analysis and Prevention*, 2004, 36:561-567.

[4] Margriet S, Stefanie H, Carmen R, Rikard F. Cyclist kinematics in car impacts reconstructed in simulations and full scale testing with Polar dummy. *Proceedings of IRCOBI Conference*, 2012, 800-812(IRC12-85), Dublin, Ireland.

[5] Maki T, Kajzer J, Mizuno K, Sekine Y. Comparative analysis of vehicle–bicyclist and vehicle–pedestrian accidents in Japan. *Accident Analysis and Prevention*, 2003, 35:927-940.

[6] Bellogi P, Lee I, Ahmed N. Car to Bicycle Side Crash Simulation. *JSAE*, 2005, 109-05:9-12.

[7] Watanabe R, Katsuhara T, Miyazaki H, Kitagawa Y, Yasuki T. Research of the relationship of pedestrian injury to collision speed, car-type, impact location and pedestrian sizes using human FE model (THUMS Version 4). *Stapp Car Crash Journal*, 2012, 56:269-321.

[8] Abe H, et al. Data Book on Mechanical properties of living cells. *Tissues and Organs. Springer-Verlag*, 1996.

[9] Yamada H. Strength of biological materials. The Williams & Wilkins Company, 1970.

[10] Takhounts E. On the development of the SIMon finite element head model. *Stapp Car Crash Journal*, 2003, SAE Paper No. 2003-22-0008.

[11] Ashley W, Kerry D, Joel S. Modeling brain injury response for rotational velocities of varying directions and magnitudes. *Annals of Biomedical Engineering*, 2012, 40:2005-2018.

[12] Marguiles S, Thibault L. A proposed tolerance criterion for diffuse axonal injury in man. *Journal of Biomechanics*, 1992, 25(8):917-923.